Dileptons, Charm and Charmonium at Finite Temperature and Chemical Potential

Ralf Rapp[*]

Cyclotron Institute and Physics Department, Texas A&M University, College Station, TX 77843-3366, USA
E-mail: `rapp@comp.tamu.edu`

We discuss how dileptons, open charm and charmonia may be utilized in heavy-ion collisions to extract information specific to hot and dense matter at finite quark chemical potential, μ_q. For each observable we briefly discuss underlying theoretical frameworks and the current status in interpreting available heavy-ion data at SPS and RHIC energies. Low-mass dileptons are particularly sensitive to baryonic medium effects in spectral modifications of the ρ meson, and may serve as an accurate measure of the fireball lifetime. In the open-charm sector, observable signals may be generated by a "critical" enhancement of scattering rates via t-channel exchange of a soft σ mode. For charmonia, finite-temperature potential models could be used to extrapolate color-screening effects to finite μ_q to facilitate a quantitative evaluation of dissociation rates in the medium.

---

[*]Speaker.

1. Introduction

Rigorous information on the QCD phase diagram, schematically depicted in Fig. 1, is scarce. At finite temperature (T) and vanishing quark chemical potential ($\mu_q = 0$), lattice QCD (lQCD) computations predict the existence of a rapid cross-over transition from hadronic matter to a Quark-Gluon Plasma at a (pseudo-) critical temperature of $T_c = (180 \pm 20)$ MeV [1, 2]. Heavy-ion collisions at SPS and RHIC energies have shown that the produced medium exhibits a high degree of thermalization and that the achieved temperatures are on the order of T_c and above. This provides a firm basis for studying QCD matter in the laboratory. At finite μ_q and vanishing T, there are compelling arguments that the high-density limit of QCD is in a color-superconducting phase (attractive quark-quark interaction plus Cooper theorem). Since this ground state, characterized by a non-vanishing diquark condensate ($\langle qq \rangle \neq 0$), is qualitatively different from the chirally broken QCD vacuum ($\langle \bar{q}q \rangle \neq 0$), it is natural to expect a first-order transition at some intermediate chemical potential, $\mu_q^c \simeq 400$ MeV. Finally, heavy atomic nuclei have been long used to quantify the properties and excitations of the finite-density ground state at $\mu_q = (m_N - E_B)/3 \simeq 310$ MeV, indicated by the square box in Fig. 1.

Heavy-ion experiments performed over a wide range of collision energies can, in principle, cover a large region of the phase diagram, cf. the "data" points in Fig. 1. In particular, as indicated
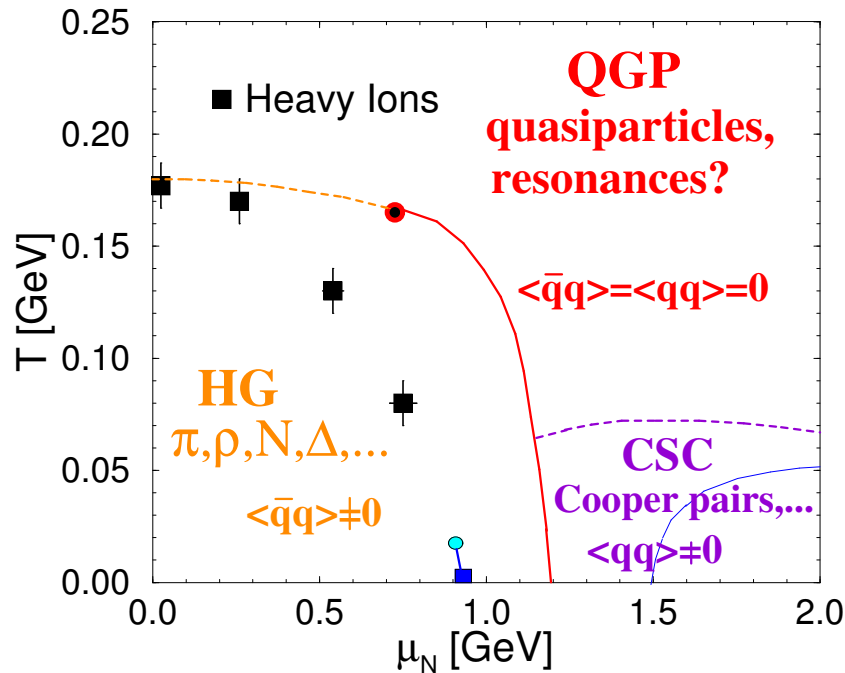
Figure 1: Schematic diagram of the QCD phase structure in the μ_q-T plane, as characterized by the lowest dimension quark condensates, i.e., the chiral quark-antiquark and the diquark one (Cooper pairs). The former is believed to prevail in the low-T and -μ_q hadronic world while the latter occurs at the Fermi surface of cold dense quark matter. Key to investigating the phase structure is the identification of the relevant excitations in the respective phases, as indicated in the figure. The "data" points are extracted from hadro-chemical analysis of the final state observed in heavy-ion collisions [3, 4].

above, one ought to be able to determine phase changes, down to temperatures of about 100 MeV where the critical chemical potential may be around $\mu_q^c \simeq 400$ MeV (it is, however, questionable whether heavy-ion experiments can reach into the color-superconducting phases, unless the zero-temperature quark pairing gap is well above 100 MeV [5]; even if so, equilibration appears to be unlikely. More likely could be the production of the so-called quarkyonic phase [6] which may extend to higher T). Of special interest is the occurrence of a critical second-order endpoint, whose existence is suggested by the cross-over transition found in finite-T lQCD and the putative 1. order transition at $T = 0$. Suitable observables to study the QCD phase structure in heavy-ion collisions (HICs) may be roughly divided into two categories: (1) bulk observables driven by the equation of state (EoS), including collective flow patterns of the most abundant particles (π, K, p) or fluctuation observables in p_T spectra and hadrochemistry; (2) "microscopic" probes associated with specific quantum-number channels, e.g., the vector current coupling to photons and dileptons. In some instances the physical origin of type (1) and (2) observables is closely related. Electric-charge fluctuations, e.g., are governed by the electromagnetic (EM) susceptibility, $\chi_{\rm em}$, which can be expressed as the screening limit of the static EM correlation function, $\langle Q^2 \rangle - \langle Q \rangle^2 = \chi_{\rm em} = \Pi_{\rm em}(q_0 = 0, q \to 0)$, while photon and dilepton spectra are directly proportional to the imaginary part of $\Pi_{\rm em}$, as discussed below.

In this paper we focus on microscopic probes as realized via dileptons, charm and charmonia. Corresponding observables are often associated with "hard probes", due to a large momentum transfer associated with their initial production (e.g., $|q^2| \geq 4m_c^2 \simeq 6$ GeV^2). We will argue, however, that all of the above 3 probes can provide valuable information on relatively "soft" modes in the medium, at the temperature scale or below. For dileptons (Sec. 2), this relates to the in-medium ρ-meson spectral function as reflected in thermal radiation at low invariant masses ($M \sim \mathscr{O}(T) \leq m_\rho$). In the open-charm sector (Sec. 3), one can study mechanisms of thermalization or, more generally, transport properties within a diffusion equation via modifications of charmed hadron p_T spectra and elliptic flow (governed by elastic scattering at typical momentum transfers $|q| \sim \mathscr{O}(gT)$). Finally, for charmonia (Sec. 4), the key to understanding their in-medium bound-state properties lies in color-screening effects (at the Debye scale $m_D \sim \mathscr{O}(gT)$) as well as inelastic dissociation reactions (at the binding-energy scale). In each sector, based on current insights, we will try to identify promising directions of future investigations specific to the situation of finite μ_q and/or the putative critical point. Concluding remarks are collected in Sec. 5.

2. Low-Mass Dileptons: ρ-Meson Spectroscopy

The basic quantity to calculate thermal emission spectra of EM radiation from hot and dense matter is the retarded correlation function of the hadronic EM current, $j_{\rm em}^\mu$,

$$\Pi_{\rm em}^{\mu\nu}(M, q; \mu_B, T) = -i \int d^4x \, e^{iq \cdot x} \, \Theta(x_0) \, \langle [j_{\rm em}^\mu(x), j_{\rm em}^\nu(0)] \rangle_T \ . \tag{2.1}$$

Its imaginary part (EM spectral function) directly figures into the differential production rates of dileptons (l^+l^-) and photons (γ),

$$\frac{dN_{ll}}{d^4x d^4q} = -\frac{\alpha_{\rm em}^2}{\pi^3} \frac{L(M)}{M^2} \, f^B(q_0; T) \, \mathrm{Im}\, \Pi_{\rm em}(M, q; \mu_B, T) \tag{2.2}$$

$$q_0 \frac{dN_\gamma}{d^4x d^3q} = -\frac{\alpha_{\text{em}}}{\pi^2} f^B(q_0;T) \, \text{Im} \, \Pi_{\text{em}}(M=0,q;\mu_B,T) \,, \qquad (2.3)$$

respectively (f^B is the thermal Bose distribution and $L(M)$ a final-state lepton phase-space factor relevant close to the dilepton threshold). In the vacuum, the low-mass regime ($M \leq 1$ GeV) of Π_{em} is essentially saturated by the light vector mesons ρ, ω and ϕ. Within the vector-dominance model (VDM) the EM spectral function is directly proportional to the vector-meson spectral functions,

$$\text{Im} \, \Pi_{\text{em}} \sim [\text{Im} \, D_\rho + \frac{1}{9}\text{Im} \, D_\omega + \frac{2}{9}\text{Im} \, D_\phi] \,. \qquad (2.4)$$

Thus, if VDM remains valid in the medium (see, e.g., Ref. [7] for an alternative scheme), low-mass dilepton spectra mostly probe in-medium modifications of the ρ meson, which have been studied rather extensively in the literature, see, e.g., Refs. [8, 9] for recent reviews.

It turns out that low-mass thermal EM radiation in HICs dominantly emanates from the hadronic phases of the collisions, even at RHIC energies [10]. It is therefore in order to study hadronic medium effects on the ρ propagator,

$$D_\rho(M,q;\mu_B,T) = [M^2 - m_\rho^{(0)^2} - \Sigma_{\rho\pi\pi} - \Sigma_{\rho B} - \Sigma_{\rho M}]^{-1} \,, \qquad (2.5)$$

encoded in selfenergy insertions, Σ_ρ, induced by interactions with particles in the heat bath. These may be classified as (a) medium modifications of the pion cloud, $\Sigma_{\rho\pi\pi}$, due to pion rescattering (most notably on baryons) and thermal Bose enhancement [11]; (b) direct ρ-baryon couplings [12], e.g., $\rho + N \rightarrow \Delta, N(1520), N(1720)$, etc.; (c) direct interactions of the ρ with mesons, e.g., $\rho + \pi \rightarrow \omega, a_1, ...$ or $\rho + K \rightarrow K_1, ...$ etc. [13]. The interactions are usually modeled by effective hadronic Lagrangians which satisfy basic constraints from EM gauge invariance and (mostly for pions) chiral symmetry. The free parameters (coupling constants and formfactor cutoffs to account for finite-size effects) can be constrained empirically by partial decay rates (e.g., $a_1 \rightarrow \pi\rho, \pi\gamma$) or, more comprehensively, scattering data (e.g., $\pi N \rightarrow \rho N$ or photo-absorption cross sections). The left panel of Fig. 2 shows an in-medium ρ spectral functions [14] including all of the above components under conditions roughly resembling HICs at the SPS. A strong broadening with increasing matter density and temperature occurs, melting the resonance when extrapolated toward the phase boundary region. The large low-mass enhancement becomes much more apparent in the dilepton production rate, due to the Bose factor and photon propagator in eq. (2.2), cf. right panel of Fig. 2. At $M \simeq 0.4$ GeV, an order of magnitude enhancement over the rate from free $\pi\pi$ annihilation is predicted. Also note that the divergence of the rate for $M \rightarrow 0$ is required to produce a finite photon production rate, eq. (2.3). Plotting the rate in terms of the 3 individual selfenergy contributions as introduced above, one clearly recognizes the prevalence of the baryon-driven medium effects. This may seem surprising since at SPS energies the observed pion-to-baryon ratio is about 5:1. However, in the interacting medium, most of the pions are "stored" in excited (meson and baryon) resonances; e.g., at $(\mu_B,T)=(240,160)$ MeV, the total baryon density, $\rho_B \simeq 0.8\rho_0$ is quite comparable to the direct pion density, $\rho_\pi \simeq 0.9\rho_0$ ($\rho_0 = 0.16$ fm^{-3}).

An application of the ρ spectral function to recent NA60 low-mass dimuon data in In-In collisions at SPS [15] is shown in the left panel of Fig. 3. Upon convoluting the EM emission rates over an expanding fireball, the excess radiation is well described by the predicted in-medium ρ
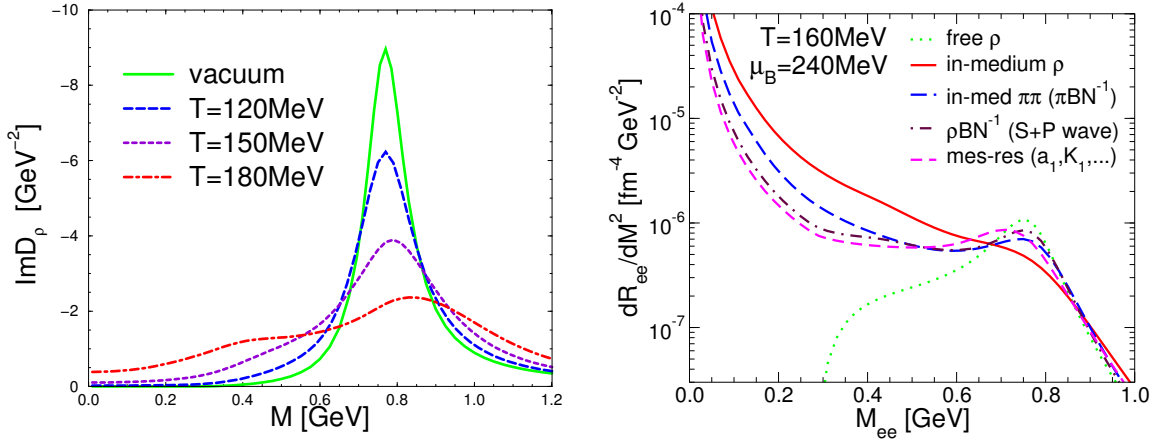
Figure 2: Left panel: ρ-meson spectral function in hot and dense hadronic matter at fixed $\mu_B = 3\mu_q = 330$ MeV (corresponding to baryon densities $\rho_B/\rho_0 = 0.1, 0.7, 2.6$ at $T = 120, 150, 180$ MeV, respectively) and 3-momentum $q = 0.3$ GeV [14]. Right panel: 3-momentum integrated thermal dielectron rates in the isovector channel using the vacuum (dotted line) and full in-medium (solid line) ρ spectral function; the long-dashed, dash-dotted and short-dashed curves only include in-medium selfenergies due to either the in-medium pion cloud ($\Sigma_{\rho\pi\pi}$) or direct ρ-baryon interactions ($\Sigma_{\rho B}$) or direct ρ-meson interactions ($\Sigma_{\rho M}$), respectively (the latter 2 include the free pion cloud as well).

line shape (QGP and primordial contributions are subleading) [16], see Refs. [17, 18, 19] for alternative calculations. This is also true for the excess dielectron data reported for central Pb-Au by CERES/NA45 [20]. One can quantify the ρ broadening by an approximate average width which amounts to $\bar{\Gamma}_\rho^{med} \simeq (350\text{-}400)$ MeV $\simeq 3\,\Gamma_\rho^{vac}$, realized at a representative temperature of $\bar{T} \simeq 150\text{-}160$ MeV, cf. right panel of Fig. 3. This inevitably implies that, toward T_c, the ρ's in-medium width becomes comparable to its mass, i.e., the resonance has indeed melted. The absolute yield of
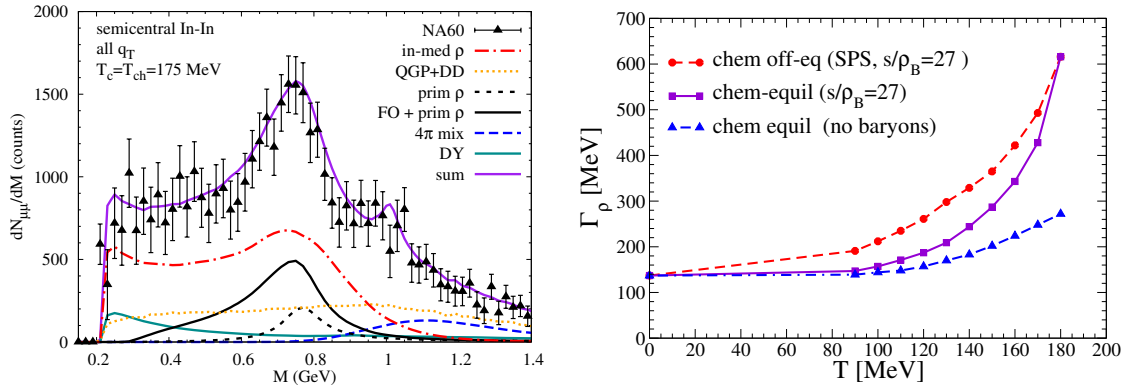
Figure 3: Left panel: dimuon invariant-mass spectra (including experimental acceptance) in semicentral In-In collisions at SPS energies ($E_{lab} = 158$ AGeV); NA60 data [15] are compared to theoretical calculations based on the in-medium ρ spectral function shown in Fig. 2. Right panel: in-medium ρ width as a function of temperature along isentropic trajectories in the phase diagram starting from chemical equilibrium at $(T, \mu_B) = (175, 230)$ MeV (dots: fixed hadrochemistry including chemical potentials for pions, kaons, etc.; squares: chemical equilibrium; triangles: without baryonic medium effects).
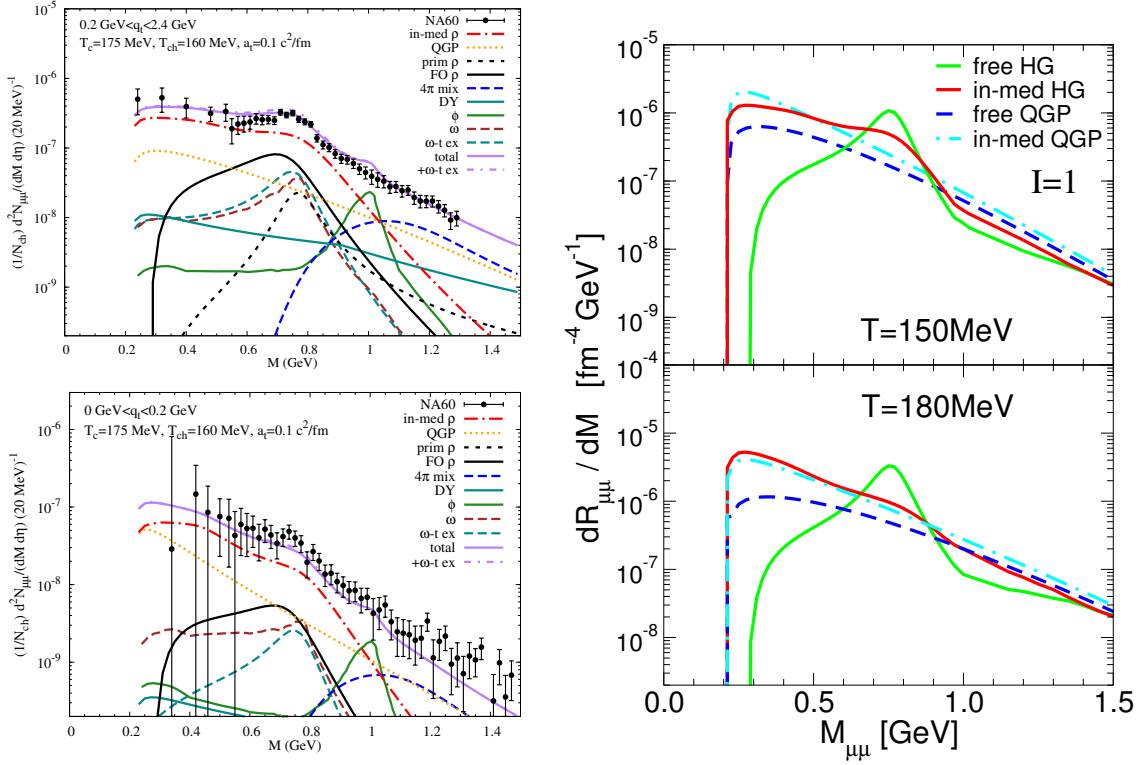
Figure 4: Left panel: acceptance-corrected dimuon invariant-mass spectra in semicentral In(158 AGeV)-In [21, 22] for transverse pair momenta $q_t = 0.2$-2.4 GeV (upper left) and $q_t = 0$-0.2 GeV (lower left). Right panel: 3-momentum integrated dimuon thermal emission rates in the isovector (ρ) channel at a baryon chemical potential representative for SPS energies ($\mu_B = 330$ MeV) [14].

the excess radiation is quite sensitive to the total fireball lifetime, enabling a remarkably accurate measurement of the fireball lifetime for semicentral In-In collision, $\tau_{FB} \simeq (6.5 \pm 1)$ fm/c. This tool could become invaluable for detecting significant lifetime changes when approaching the critical point and/or moving into the first-order regime with an extended mixed phase (of course, it only works if the in-medium spectral shape is under sufficient theoretical control).

The NA60 collaboration has recently taken another step forward by fully correcting their data for experimental acceptance [21, 22]. Upon integrating over transverse momentum, the resulting invariant-mass spectra, $dN_{\mu\mu}/dMdy$, do justice to the notion of Lorentz-*invariance*, i.e., transverse flow effects have been eliminated. Thus, one is essentially looking at the (average) emission rate from the medium, multiplied by the emitting 4-volume, cf. left panels in Fig. 4. This provokes a direct comparison to the theoretical input rates based on Ref. [14], augmented by the muon phase-space factor, $L(M)$, shown in the right panel of Fig. 4 for two temperatures. The resemblance of the in-medium hadronic rates and the NA60 spectra is rather astonishing, both in slope and shape. The former can, in principle, serve as a true thermometer, i.e. free from blue-shift contamination due to transverse flow. Essential to these arguments is the prevalence of thermal radiation in the excess spectra which is borne out of (i) the theoretical calculations, and (ii) the complete lack of polarization in the measured angular distribution of the muon pairs [23]. The good overall agreement of theory and data furthermore corroborates that VDM stays intact even close to the
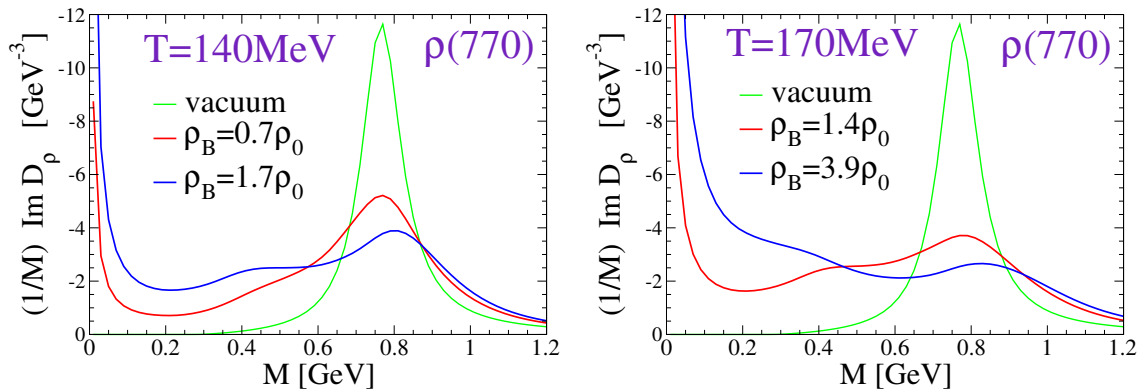
Figure 5: ρ-meson spectral functions, weighted by a factor of inverse mass as figuring into the 3-momentum integrated dilepton rate, at two temperatures and for baryon densities representative for full SPS energy (red lines) and CBM energies (blue lines).

phase boundary (the data also indicate that the φ does not radiate dileptons in the hadronic phase but decouples earlier [24, 25]; this is, in fact, consistent with its relatively soft p_T spectra).

The importance of baryon-driven medium effects in the interpretation of the SPS low-mass dilepton data naturally calls for studies at lower collisions energies where even larger baryon compression may be achieved. Hadronic many-body calculations identify the mass regime around $M \simeq 0.2$ GeV as the most sensitive one in the ρ spectral function, with up to a factor of ∼2 enhancement under conditions expected at the Compressed Baryonic Matter (CBM) experiment relative to full SPS energy. A first glimpse at such an effect may have been seen by CERES/NA45 in a 40 AGeV Pb-Au run [26]. We also note that the low-mass excess reported by PHENIX in Au-Au collisions at $\sqrt{s_{NN}}$=200 AGeV [27] currently evades a theoretical explanation.

A direct way to study baryon effects is provided by cold nuclear matter, i.e., in atomic nuclei. The advantage over heavy-ion experiments obviously lies in the essentially static matter environment, which, however, is limited by nuclear saturation density (ρ_0) and also exhibits significant spatial gradients. Nevertheless, the predicted medium effects on the ρ spectral function are appreciable even at half saturation density, at least at small 3-momentum relative to the nuclear rest frame, see left panel of Fig. 6 [14, 28]. As in HICs, the dilepton final state is the cleanest way to probe medium effects. The initial state in nuclear production experiments is, however, rather different: the ρ has to be created by an external excitation (cf. right panel of Fig. 6), as compared to an approximately thermal medium in HICs. Thus, a good knowledge of the production process is mandatory, which can be tested with proton targets. Two additional complications arise: (a) an in-medium broadening leads to a reduction in the dilepton to hadronic branching ratio, thus reducing the signal (in HICs the ρ is "continuously" regenerated in the interacting medium); (b) to provide the mass of the ρ a rather energetic incoming particle is needed which usually implies that the ρ carries significant 3-momentum; this enhances surface and/or escape effects thus reducing the in-medium signal as well. The latter point is presumably best dealt with using a photon beam where all the incoming energy can be converted into mass. Photo-production of dileptons has recently been studied by the CLAS collaboration at Jefferson Lab (JLab) using a variety of nuclear targets [29],
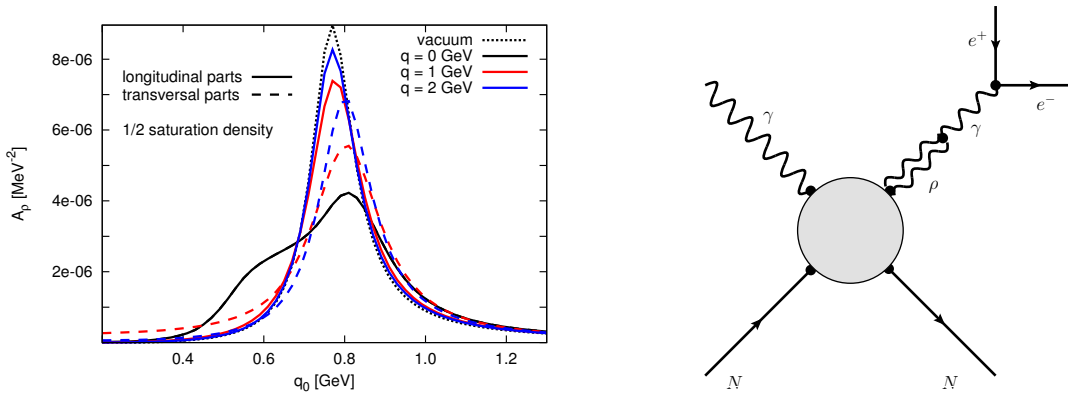
Figure 6: Left panel: in-medium ρ spectral function in cold nuclear matter at half saturation density for various 3-momenta (for $q>0$, transverse and longitudinal modes split). Right panel: elementary amplitude for ρ photo-production on the nucleon [28].
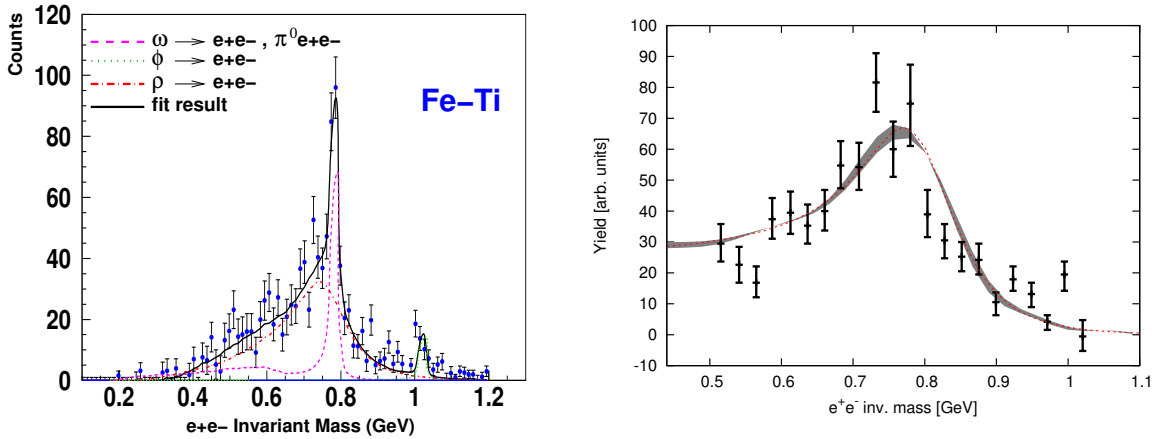
Figure 7: Dilepton spectra measured in nuclear photo-production by CLAS at JLab [29], including transport model calculations [30] for the decays of light vector mesons ρ, ω and ϕ. Right panel: CLAS "excess spectra" compared to calculations [28] using the same ρ spectral function as for the NA60 data in Figs. 3, 4.

with an incoming photon spectrum ranging over $E_\gamma \simeq (1\text{-}3.5)$ GeV. The left panel of Fig. 7 shows the dilepton signal from iron targets, compared to Boltzmann transport calculations [30] for ρ, ω and ϕ decays. Since the ω and ϕ peaks are essentially unaffected by the medium (and well concentrated in mass), their contribution can be subtracted from the spectrum (much like for the NA60 data) leading to an "excess" signal as shown by the data in the right panel of Fig. 7. Breit-Wigner fits have been applied resulting in a moderate ρ broadening to $\Gamma_\rho^{\text{med}} \simeq 220$ MeV [29]. The ρ spectral function used at SPS has been applied to the CLAS experiment in combination with a realistic elementary production amplitude and a schematic modeling of the spatial propagation, accounting for the production kinematics and nuclear density profile [28]. The CLAS data are reasonably well described; for the Fe target the typical densities and 3-momenta probed in the spectral function are $\bar{\rho} \simeq 0.5\rho_0$ and $\bar{q} \simeq 2$ GeV. The latter are the main reason for moderating the medium effects in the CLAS data (recall left panel of Fig. 6). However, at high momenta additional medium effects not included in the spectral function of Ref. [14] may occur, see, e.g., the discussion in Ref. [31].
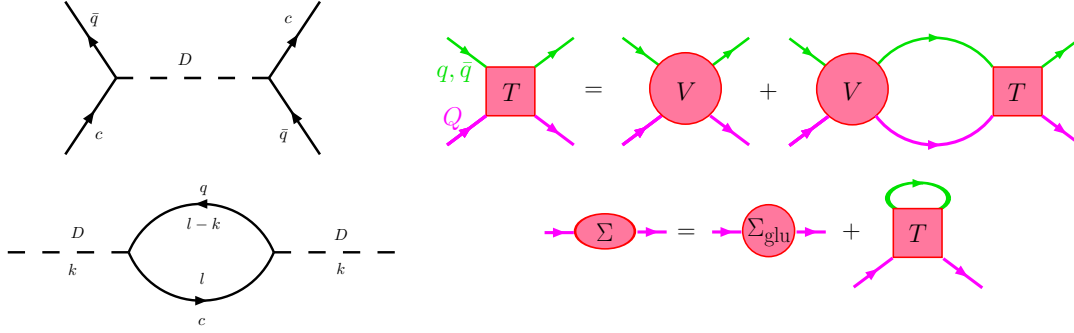
Figure 8: Left panels: *c*-quark scattering off light antiquarks via *s*-channel *D*-mesons (upper panel) and pertinent *D*-meson selfenergy (lower panel) within the effective resonance model in the QGP [33]. Right panels: selfconsistent Brueckner scheme for heavy quarks in the QGP based on an in-medium heavy-light *T*-matrix with interaction potential *V* (upper panel) and pertinent HQ selfenergy (lower panel) [44].

3. Open Charm and Transport

The masses of charm and bottom quarks (and hadrons) are much larger than the typical temperatures realized in heavy-ion collisions at SPS and RHIC, $m_Q \gg T$ ($Q=b,c$). Furthermore, a typical momentum transfer from the heat bath, $|q^2| \simeq T^2$, is parametrically smaller than the thermal momentum of *c* and *b* quarks, $p^2 \sim 3m_Q T \gg |q^2|$. Thus a diffusion approximation to the Boltzmann equation becomes applicable leading to a Fokker-Planck equation [32, 33, 34, 35],

$$\frac{\partial f_Q}{\partial t} = \gamma \frac{\partial (p f_Q)}{\partial p} + D \frac{\partial^2 f_Q}{\partial p^2} \, , \tag{3.1}$$

for the heavy-quark (HQ) phase-space distribution, f_Q. The scattering rate, γ, and momentum diffusion coefficient, D, are related via the Einstein relation, $T = D/(\gamma m_Q)$. Applications to RHIC data revealed that perturbative QCD (pQCD) elastic scattering is insufficient to generate the observed elliptic flow, even with a strong coupling constant as large as $\alpha_s = 0.4$, supporting the notion of a strongly coupled QGP (sQGP). At strong coupling, diagrams with large contributions have to be resummed, possibly leading to the appearance of collective modes (bound states or resonances). In this spirit, the effective resonance model for *c*- and *b*-quark scattering through in-medium *D* and *B* meson has been introduced [33]. The pertinent *s*-channel diagrams are displayed in the left panels of Fig. 8. An approximately 4-fold decrease of the HQ thermalization time, $\tau_Q = \gamma^{-1}$, has been found relative to pQCD. When implemented into relativistic Langevin simulations within an expanding fireball for Au-Au collisions at RHIC [36], the recent data on suppression and elliptic flow of semileptonic decay electrons are fairly well described [38, 39], cf. left panel of Fig. 9 (see also Refs. [41, 42, 43]). Heavy-light quark coalescence in the hadronization process at T_c plays a significant role in increasing *both* R_{AA} and v_2.

One may ask whether resonant HQ interactions in the QGP can be understood more microscopically. This question has been studied using a heavy-light quark *T*-matrix equation [44],

$$T_{qQ} = V_{qQ} + V_{qQ} G_{qQ} T_{qQ} \, , \tag{3.2}$$

diagrammatically depicted in the upper right panel of Fig. 8. The key input is the driving kernel (potential), V_{qQ}, which has been assumed to coincide with the static HQ internal energy computed
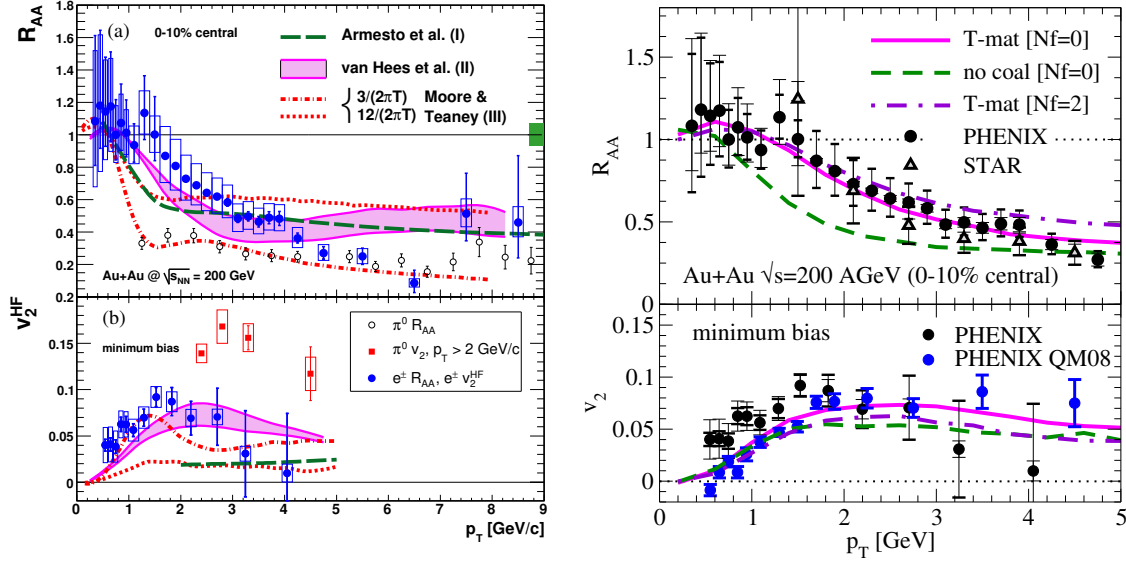
Figure 9: RHIC data [38, 39, 40] for the nuclear modification factor (upper panels) and elliptic flow (lower panels) of HQ decay electrons in Au-Au collisions, compared to theory. Left panels: relativistic Langevin simulations using upscaled pQCD elastic scattering cross sections (short-dashed and dash-dotted line) [34] or effective resonances+pQCD elastic scattering (bands) [36], and radiative energy-loss calculations (long-dashed lines) [37]. Right panels: Langevin simulations with T-matrix+pQCD elastic interactions [44] using internal energies from quenched (solid line) and N_f=2 (dash-dotted line) thermal lQCD [45]; for the dashed lines hadronization via heavy-light quark coalescence at T_c is switched off.

in thermal lQCD, augmented by relativistic corrections due to color-magnetic current-current interactions. In addition to the color-singlet channel, the Q-$\bar{q}$ and Q-q interactions in the color-octet, -antitriplet and -sextet channels have been estimated using Casimir scaling. It turns out that the interaction strength is concentrated in the attractive singlet and antitriplet channels, supporting Feshbach-like meson and diquark resonances close to the q-Q threshold up to temperatures of $\sim$1.7 T_c and $\sim$1.4 T_c, respectively. Compared to the resonance model, the HQ interaction in the T-matrix approach of similar strength close to T_c, but weakens at higher T due to color-screening in the potential which dissolves the resonances. An open problem remains the nonperturbative treatment of HQ-gluon interactions. The application of the T-matrix approach to RHIC electron data looks promising (right panels in Fig. 9), but significant uncertainties remain which currently inhibit definite conclusions about the microscopic origin of HQ diffusion.

What effects can be expected for charm-quark diffusion at finite μ_q, relevant for CBM energies and a RHIC energy scan? The effective resonance model suggests that, in a quark-dominated environment, anticharm quarks ($\bar{c}+q \to \bar{D}$) interact more frequently than charm quarks ($c+\bar{q} \to D$). However, in the T-matrix approach, scattering via (anti-) diquarks, cq and $\bar{c}\bar{q}$, is equally important, thus washing out the asymmetry. Moreover, in the hadronic phase, the baryon excess favors D-meson scattering via $\Lambda_c N^{-1}$ excitations over its antiparticle conjugate. A promising possibility could be the development of the σ soft mode close to the critical point, which is particularly pronounced in the spacelike regime [46]. *If* charm quarks couple to the σ, their t-channel exchange cross section with light quarks (and hadrons) could be "critically" enhanced leaving observable traces in D-meson p_T spectra and v_2 (see Ref. [47] for a related study in the light-quark sector).
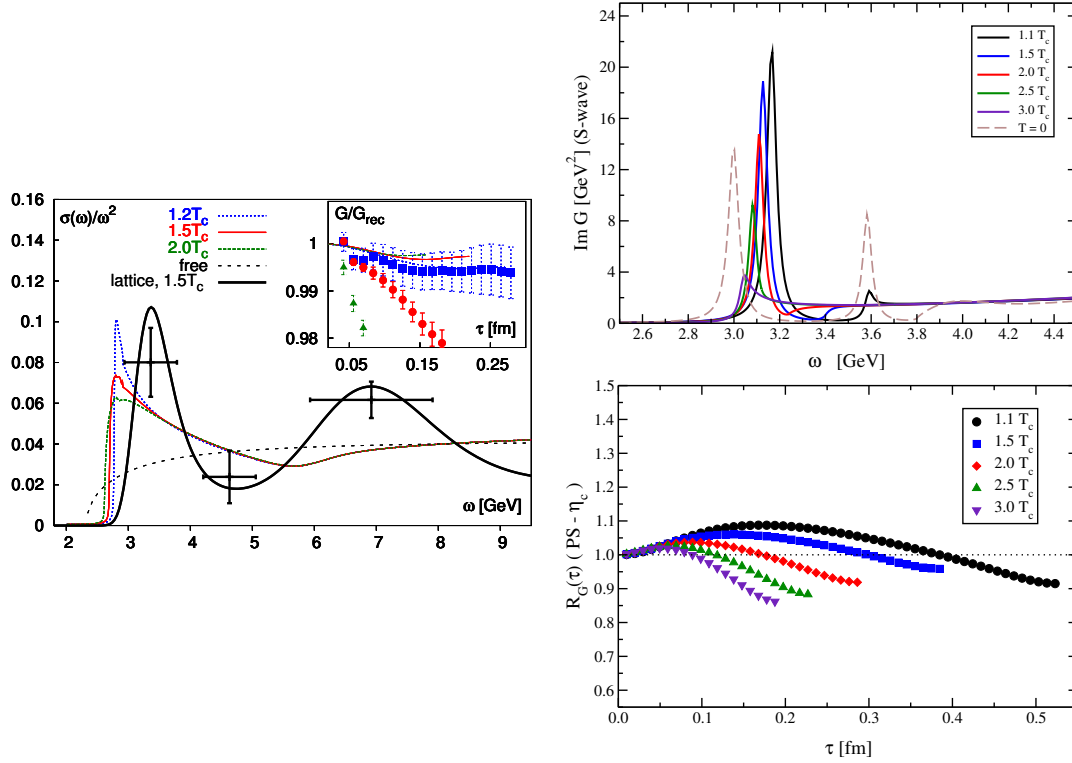
Figure 10: *S*-wave c-$\bar{c}$ spectral functions and Euclidean-time correlators (normalized with a "reconstructed" correlator, $R_G(\tau) \equiv G(\tau)/G_{\text{rec}}(\tau)$) using a HQ potential close to the lQCD free energy (left panels) [48] or corresponding to the lQCD internal energy (right panels) [49].

4. Charmonia: Screening and Dissociation

The dissolution temperature of charmonia in medium largely depends on two mechanisms: color-screening of the inter-quark force and inelastic dissociation reactions. While the former largely governs the Q-$\bar{Q}$ binding energy, ε_B (via spacelike gluon exchange), the latter determines the inelastic width, $\Gamma_\psi^{\text{inel}}$, of the bound-state (via dissociation reactions with timelike (on-shell) partons in the heat bath). Within a schematic pole ansatz, both mechanisms figure into the charmonium spectral function as

$$\sigma_\psi(\omega) \sim \text{Im}\, D_\psi(\omega) \sim \text{Im}\, [\omega - 2m_c^* + \varepsilon_B + i\Gamma_\psi/2]^{-1} \tag{4.1}$$

(a pole ansatz applies to a well-defined bound-state/resonance). Note the dependence on the in-medium c-quark mass, m_c^*, and that the total width, Γ_ψ, includes contributions from elastic scattering as well. However, as we will see below, binding energies and dissociation reactions mutually influence each other.

Recent years have seen a revival of potential models to evaluate in-medium quarkonium properties [48, 49, 50, 51, 52, 53]. This was largely spurred by the hope that the input potential can be taken in a model-independent way from the HQ free energy computed in thermal lQCD, and that resulting spectral functions can be discriminated via comparisons to Euclidean correlation functions independently computed in lQCD. There is, however, an ongoing controversy as to which

11
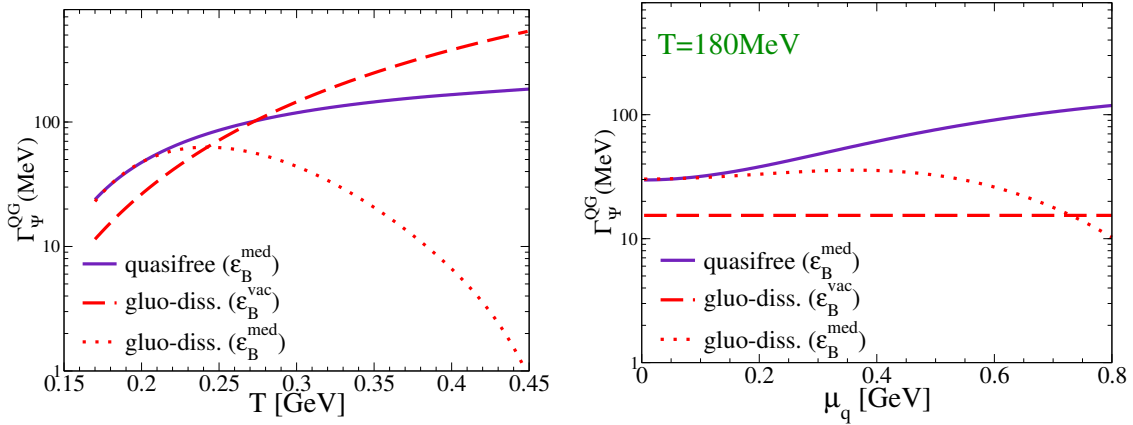
Figure 11: J/ψ dissociation rate (=inelastic width) in a QGP as a function of T (at μ_q=0, left panel) and μ_q (at T=180 MeV, right panel) for gluo-dissociation ($g + J/\psi \to c + \bar{c}$) and quasifree destruction ($p + J/\psi \to p + c + \bar{c}$ with $p = q, \bar{q}, g$) with vacuum and in-medium reduced J/ψ binding energy.

quantity to identify with a potential (free vs. internal energy), and concerning the gauge variance of the projection on the color-singlet channel [54]. More quantitatively, the current situation is illustrated in Fig. 10. Roughly speaking, when the singlet free energy, $F^1_{Q\bar{Q}}(r,T)$, is used as potential, ground-state charmonia dissolve at temperatures below $1.5\,T_c$ (left panel) [48]. On the other hand, with the internal energy, $U^1_{Q\bar{Q}} = F^1_{Q\bar{Q}}(r,T) + TS^1_{Q\bar{Q}}(r,T)$ ($S_{Q\bar{Q}}$: entropy), a J/ψ peak in the spectral function can survive up to 2.5-3 T_c (upper right panel) [49]. The spectral functions have been used to calculate temporal Euclidean correlation functions,

$$G_\psi(\tau, p; T) = \int\limits_0^\infty d\omega \, \sigma_\psi(\omega, p; T) \, \frac{\cosh[(\omega(\tau - 1/2T)]}{\sinh[\omega/2T]} \, , \tag{4.2}$$

which are usually normalized to a "reconstructed" correlator, $G_{\rm rec}$, computed with a vacuum spectral function (but identical finite-temperature kernel in eq. (4.2)). Surprisingly, both weak and strong-binding scenarios for the spectral function result in correlator ratios which are around one and depend weakly on temperature (compatible with lQCD results [55, 56, 57]), cf. inset in the left panel and lower right panel of Fig. 10. The reason for this "redundancy" is the underlying effective quark mass, which is calculated from the asymptotic value of the HQ free or internal energy, $m_c^* = m_c^0 + \Delta m_c$ with $2\Delta m_c = F(r \to \infty, T)$ or $U(r \to \infty, T)$. For the free energy, Δm_c is substantially reduced from its vacuum value, thus lowering the in-medium $c\bar{c}$ threshold considerably; this compensates for the lack of a bound state in providing low-energy strength in the spectral function to ensure a stable correlator ratio. For the internal energy, Δm_c is significantly larger which, together with a stronger binding, leads to an essentially stable J/ψ peak position and thus a roughly stable T-dependence of the correlator ratio. More work is needed to disentangle these two scenarios. Finite-width effects on the correlators have received rather little attention thus far, but they seem to further stabilize the T-dependence [49]. If a reliable understanding of quarkonium correlators in the QGP at $\mu_q = 0$ in terms of potential models can been established, it might serve as a benchmark to extrapolate, e.g., color-screening effects to finite μ_q.

The dissociation width of heavy quarkonia in medium is pivotal for a quantitative description of suppression (and regeneration!) reactions in HICs. The prevalent dissociation mechanism in the

QGP depends on the binding energy of the bound state [58, 59, 60, 61], cf. left panel of Fig. 11. For large binding, $\varepsilon_B \sim 3T$, thermal-gluon absorption is most efficient, $g + J/\psi \to c + \bar{c}$ (and formally the process to leading-order in α_s). For small binding, $\varepsilon_B < T$, the phase space for gluo-dissociation shrinks leading to a decrease in its rate with T. Thus, "quasi-free" dissociation, $p + J/\psi \to p + c + \bar{c}$, albeit formally of higher order in α_s, takes over. Note that the quasi-free process can be induced by both gluons and anti-/quarks ($p = q, \bar{q}, g$). As a consequence, at finite μ_q, quasifree dissociation is additionally enhanced over gluo-dissociation due to an increasing abundance of thermal quarks, cf. right panel of Fig. 11 [62].

5. Conclusions

Instead of a formal summary of this paper, let us reiterate what we find the most promising perspectives regarding the finite-μ_q dependence of dileptons and charm/onia at this point. For low-mass dileptons, we have identified the mass region around $M \simeq 0.2$ GeV as the most sensitive one for baryon-driven medium effects. In addition, with a good knowledge of the in-medium spectral shape of the EM correlator, the dilepton yield can finally be used for an accurate determination of the fireball lifetime in HICs, which might be useful in detecting (the onset of) an extended quark-hadron mixed phase. For open charm, a "critical" enhancement of σ exchange in c-quark or D-meson scattering in the vicinity of the critical point may occur, potentially affecting transport properties in an observable way (p_t spectra and elliptic flow). For charmonia, a hope is to establish the validity of finite-T potential models and extrapolate them to finite μ_q, augmented by microscopic calculations of dissociation rates. These developments are particularly exciting in view of future tests in several heavy-ion programs around the world.

Acknowledgments

References

[1] M. Cheng *et al.*, *Phys. Rev. D* **77** (2008) 014511 [`0710.0354[hep-lat]`].

[2] Y. Aoki, Z. Fodor, S.D. Katz and K.K. Szabo, *Phys. Lett. B* **643** (2006) 46 [`hep-lat/0609068`].

[3] P. Braun-Munzinger, K. Redlich and J. Stachel (2003), in R.C. Hwa, X.N. Wang (editors), *Quark-gluon plasma* **vol. 3** (World Scientific, 2004) p. 491, [`nucl-th/0304013`].

[4] F. Becattini *et al.*, *Phys. Rev. C* **69** (2004) 024905 [`hep-ph/0310049`].

[5] R. Rapp, T. Schafer, E. V. Shuryak and M. Velkovsky, *Annals Phys.* **280** (2000) 35 [`hep-ph/9904353`].

[6] L. McLerran and R. D. Pisarski, *Nucl. Phys. A* **796** (2007) 83 [`0706.2191[hep-ph]`].

[7] M. Harada and K. Yamawaki, *Phys. Rept.* **381** (2003) 1 [hep-ph/0302103].

[8] R. Rapp, J. Wambach and H. van Hees, to appear in *Landolt Börnstein* vol. **1-23A** [0901.3289[hep-ph]].

[9] S. Leupold, V. Metag and U. Mosel, LANL arXiv:0907.2388[nucl-th].

[10] G. David, R. Rapp and Z. Xu, *Phys. Rept.* **462** (2008) 176 [nucl-ex/0611009].

[11] M. Urban, M. Buballa, R. Rapp and J. Wambach, *Nucl. Phys. A* **673** (2000) 357 [nucl-th/9910004].

[12] B. Friman and H.J. Pirner, *Nucl. Phys. A* **617** (1997) 496 [nucl-th/9701016].

[13] R. Rapp and C. Gale, *Phys. Rev. C* **60** (1999) 024903 [hep-ph/9902268].

[14] R. Rapp and J. Wambach, *Eur. Phys. J. A* **6** (1999) 415 [hep-ph/9907502].

[15] R. Arnaldi *et al.* [NA60 Collaboration], *Phys. Rev. Lett.* **96** (2006) 162302 [nucl-ex/0605007].

[16] H. van Hees and R. Rapp, *Nucl. Phys. A* **806** (2008) 339 [0711.3444[hep-ph]].

[17] K. Dusling and I. Zahed, *Phys. Rev. C* **80** (2009) 014902 [hep-ph/0701253].

[18] J. Ruppert *et al.*, *Phys. Rev. Lett.* **100** (2008) 162301 [0706.1934[hep-ph]].

[19] E.L. Bratkovskaya, W. Cassing and O. Linnyk, *Phys. Lett. B* **670** (2009) 428 [0805.3177[nucl-th]].

[20] D. Adamova *et al.* [CERES/NA45 Collaboration], *Phys. Lett. B* **666** (2008) 425 [nucl-ex/0611022].

[21] R. Arnaldi *et al.* [NA60 Collaboration], *Eur. Phys. J. C* **59** (2009) 607 [0810.3204[nucl-ex]].

[22] R. Arnaldi *et al.* [NA60 Collaboration], *Eur. Phys. J. C* **61** (2009) 711 [0812.3053[nucl-ex]].

[23] R. Arnaldi *et al.* [NA60 Collaboration], *Phys. Rev. Lett.* **102** (2009) 222301 [0812.3100[nucl-ex]].

[24] D. Adamova *et al.* [CERES/NA45 Collaboration], *Phys. Rev. Lett.* **96** (2006) 152301 [nucl-ex/0512007].

[25] R. Arnaldi *et al.* [NA60 Collaboration], arXiv:0906.1102[hep-ex].

[26] D. Adamova *et al.* [CERES/NA45 Collaboration], *Phys. Rev. Lett.* **91** (2003) 042301 [nucl-ex/0209024].

[27] S. Afanasiev et al. [PHENIX Collaboration], arXiv:0706.3034 [nucl-ex].

[28] F. Riek, R. Rapp, T.S. Lee and Y. Oh, *Phys. Lett. B* **677** (2009) 116 [0812.0987[nucl-th]].

[29] M.H. Wood *et al.* [CLAS Collaboration], *Phys. Rev. C* **78** (2008) 015201 [0803.0492[nucl-ex]].

[30] P. Mühlich *et al.*, *Phys. Rev. C* **67** (2003) 024605 [nucl-th/0210079].

[31] R. Rapp and J. Wambach, *Adv. Nucl. Phys.* **25** (2000) 1 [hep-ph/9909229].

[32] B. Svetitsky , *Phys. Rev. D* **37** (1988) 2484.

[33] H. van Hees and R. Rapp, *Phys. Rev. C* **71** (2005) 034907 [nucl-th/0412015].

[34] G.D. Moore and D. Teaney, *Phys. Rev. C* **71** (2005) 064904 [hep-ph/0412346].

[35] M.G. Mustafa, *Phys. Rev. C* **72** (2005) 014905 [`hep-ph/0412402`].

[36] H. van Hees, V. Greco and R. Rapp, *Phys. Rev. C* **73** (2006) 034913 [`nucl-th/0508055`].

[37] N. Armesto *et al.*, *Phys. Lett. B* **637** (2007) 362 [`hep-ph/0511257`].

[38] A. Adare *et al.* [PHENIX Collaboration], *Phys. Rev. Lett.* **98** (2008) 172301 [`nucl-ex/0611018`].

[39] B.I. Abelev *et al.* [STAR Collaboration], *Phys. Rev. Lett.* **98** (2007) 192301 [`nucl-ex/0607012`].

[40] D. Hornback *et al.* [PHENIX Collaboration], *J. Phys. G* **35** (2008) 104113 [`0804.4825[nucl-ex]`].

[41] B. Zhang, L.W. Chen and C.M. Ko, Phys. Rev. C **72**, 024906 (2005) [`nucl-th/0502056`].

[42] P.B. Gossiaux and J. Aichelin, *Phys. Rev. C* **78** (2008) 014904 [`0802.2525[hep-ph]`].

[43] Y. Akamatsu, T. Hatsuda and T. Hirano, *Phys. Rev. C* **79** (2009) 054907 [`0809.1499[hep-ph]`].

[44] H. van Hees, M. Mannarelli, V. Greco and R. Rapp, *Phys. Rev. Lett.* **100** (2008) 192301 [`0709.2884[hep-ph]`].

[45] O. Kaczmarek *et al.*, *Prog. Theor. Phys. Suppl.* **153** (2004) 287 [`hep-lat/0312015`].

[46] H. Fujii, *Phys. Rev. D* **67** (2003) 094018 [`hep-ph/0302167`].

[47] P. Zhuang, J. Hüfner, S.P. Klevansky and L. Neise, *Phys. Rev. D* **51** (1995) 3728.

[48] A. Mocsy and P. Petreczky, *Phys. Rev. D* **77** (2008) 014501 [`0705.2559[hep-ph]`].

[49] D. Cabrera and R. Rapp, *Phys. Rev. D* **76** (2007) 114506 [`hep-ph/0611134`].

[50] W.M. Alberico, A. Beraudo, A. De Pace and A. Molinari, *Phys. Rev. D* **75** (2007) 074009 [`hep-ph/0612062`].

[51] C.Y. Wong and H. W. Crater, *Phys. Rev. D* **75** (2007) 034505 [`hep-ph/0610440`].

[52] M. Laine, O. Philipsen and M. Tassler, *JHEP* **0709** (2007) 066 [`0707.2458[hep-lat]`].

[53] N. Brambilla, J. Ghiglieri, A. Vairo and P. Petreczky, *Phys. Rev. D* **78** (2008) 014017 [`0804.0993[hep-ph]`].

[54] O. Philipsen, Nucl. Phys. A **820** (2009) 33C [`0810.4685[hep-ph]`].

[55] S. Datta, F. Karsch, P. Petreczky and I. Wetzorke, *Phys. Rev. D* **69** (2004) 094507 [`hep-lat/0312037`].

[56] A. Jakovac, P. Petreczky, K. Petrov and A. Velytsky, *Phys. Rev. D* **75** (2007) 014506 [`hep-lat/0611017`].

[57] G. Aarts *et al.*, *Phys. Rev. D* **76** (2007) 094513 [`0705.2198[hep-lat]`].

[58] D. Kharzeev, L.D. McLerran and H. Satz, *Phys. Lett. B* **356** (1995) 349 [`hep-ph/9504338`].

[59] L. Grandchamp and R. Rapp, *Phys. Lett. B* **523** (2001) 60 [`hep-ph/0103124`].

[60] Y. Park *et al.*, *Phys. Rev. C* **76** (2007) 044907 [`0704.3770[hep-ph]`].

[61] X. Zhao and R. Rapp, *Phys. Lett. B* **664** (2008) 253 [`0712.2407[hep-ph]`].

[62] X. Zhao and R. Rapp, in preparation.